Short communication

High performance direct ethanol fuel cell with double-layered anode catalyst layer

Q. Wang [a,b], G.Q. Sun [a,*], L. Cao [a,b], L.H. Jiang [a], G.X. Wang [a],
S.L. Wang [a], S.H. Yang [a], Q. Xin [a]

[a] *Dalian Institute of Chemical Physics, Chinese Academy of Sciences, Dalian, 116023, China*
[b] *Graduate School of the Chinese Academy of Sciences, Beijing, 100039, China*

Abstract

Double-layered anode catalyst layers with two reverse configurations, which consist of 45 wt.% Pt_3Sn/C and PtRu black catalyst layers, were fabricated to improve the performance of a direct ethanol fuel cell (DEFC). The in-house 45 wt.% Pt_3Sn/C catalyst was characterized by XRD and TEM. The cross-sectional double-layered anode catalyst layer was observed by SEM. In DEFC performance test and anode linear sweep voltammetry measurement, the anode with double-layered catalyst layer exhibited better catalytic activity for ethanol electro-oxidation than those with single-layered 45 wt.% Pt_3Sn/C and PtRu black catalyst layers. In terms of anode product distribution, the DEFC with double-layered anode catalyst layer showed a higher yield of acetic acid than that with single-layered PtRu black catalyst layer and a higher yield of CO_2 than that with single-layered 45 wt.% Pt_3Sn/C catalyst layer, respectively. These results suggest that the double-layered anode catalyst layer possessed the advantages of both Pt_3Sn/C and PtRu black catalysts for ethanol electro-oxidation, and thus showed a higher ethanol electro-oxidation efficiency and DEFC performance in the practical polarization potential region.
© 2007 Elsevier B.V. All rights reserved.

Keywords: Direct ethanol fuel cell; Double-layered anode catalyst layer; Pt_3Sn/C catalyst; PtRu black catalyst

1. Introduction

In the last decade, direct ethanol fuel cell (DEFC) has attracted increasing attention because ethanol has several advantages compared with methanol, such as low toxicity and high theoretical energy density ($8.0 \, kWh \, kg^{-1}$), etc. [1,2]. However, the slow kinetics of ethanol electro-oxidation at low temperatures is still a major challenge for the research and development of DEFC. Much effort has been devoted to screen effective catalysts for ethanol electro-oxidation by the combination of electrochemical and spectroscopy techniques, such as differential electrochemical mass spectroscopy (DEMS), Fourier transform infrared spectroscopy (FTIRS), etc. [3–6]. PtRu and PtSn catalysts were widely investigated as anode catalysts in DEFC since they showed different catalytic behaviors on the ethanol dissociation and electro-oxidation [4–6,7–12]. According to the bi-functional mechanism [11,13], it is generally believed that the role of Ru in PtRu catalyst was to promote water dissociation at low potentials in ethanol electro-oxidation and thus produce the oxygenated species (e.g., adsorbed OH) to give a relatively higher yield of CO_2. When Pt was modified by Sn, the effect of CO poisoning was reduced and ethanol electro-oxidation went through the pathway of yielding acetaldehyde and finally acetic acid [8,14–16]. Wang et al. also considered that the catalysis of Pt_3Sn/C catalyst for ethanol electro-oxidation did not improve the selectivity of complete oxidation to CO_2 according to the DEMS study [17]. Until now, various preparation methods have been used to optimize the composition and structure of PtSn and PtRu catalysts with the purpose of improving their catalytic activities [7–9,11–15], however, the DEFC performance of the two catalysts is still poor and needs to be improved greatly. In view of the different catalytic properties of PtRu and PtSn catalysts towards ethanol electro-oxidation, it is interesting to investigate their combined effects on DEFC performance by fabricating an electrode using the two catalysts.

* Corresponding author. Tel.: +86 411 84379063; fax: +86 411 84379063.
  E-mail address: gqsun@dicp.ac.cn (G.Q. Sun).

In this work, double-layered anode catalyst layers with two reverse configurations were fabricated by using in-house 45 wt.% Pt₃Sn/C catalyst and commercial PtRu black catalyst. The DEFCs with both double-layered (D-L) anode catalyst layers showed a greater performance than those with single-layered (S-L) 45 wt.% Pt₃Sn/C and PtRu black catalyst layers. The prepared 45 wt.% Pt₃Sn/C catalyst was characterized by XRD and TEM, and the cross-sectional morphology of the D-L anode catalyst layer was observed by SEM. Single cell test and anode polarization measurement in combination with anode product analysis were carried out to investigate the improvement of DEFC performance and variation of product distribution.

2. Experimental

2.1. Catalyst preparation

$H_2PtCl_6 \cdot 6H_2O$ and $SnCl_2 \cdot 2H_2O$ were used as the precursors of Pt₃Sn/C catalyst. Vulcan XC-72R carbon black (Cabot Corp., $S_{BET} = 237 \, m^2 \, g^{-1}$) was served as support material. The detailed process has been described elsewhere [18]. The required amounts of $H_2PtCl_6 \cdot 6H_2O$ and $SnCl_2 \cdot 2H_2O$ and carbon powder were added to ethylene glycol solution with stirring to form a homogeneous slurry. The slurry was heated to 165 °C and kept at this temperature for 4 h in an oil bath. Then the black solid samples were filtered, washed and dried at 80 °C for 10 h in a vacuum oven. The metal loading of the catalyst on carbon was 45 wt.% (the nominal atomic ratio of Pt to Sn is 3:1, Pt₃Sn/C for short in the next paragraphs).

2.2. MEA fabrication

Preparation of anode and cathode diffusion layers on SGL GDL-20-AA carbon paper (0.19 mm thick, SGL Carbon Group, Short Hills, NJ) has been previously described [19]. The D-L anode catalyst layers consisted of Pt₃Sn/C and PtRu black catalyst layers with two reverse configurations. In the first D-L anode catalyst layer(denoted as D-L-1 anode catalyst layer), Pt₃Sn/C catalyst layer was close to the anode diffusion layer as the first layer, and PtRu black catalyst layer was adjacent to the Nafion® membrane as the second layer. To prepare the first layer, the in-house Pt₃Sn/C catalyst was mixed into a water/alcohol solution along with a 5 wt.% Nafion solution (Dupont) and the resulting mixture was ultrasonically agitated with vigorous mechanical stirring to form a homogeneous ink. The ink was then brushed onto the anode diffusion layer held on a heating table at 60 °C to form the first catalyst layer. The resulting catalyst loading was 4.5 mg cm⁻² and the Nafion content was 10 wt.%. And then 1 mg cm⁻² dry Nafion ionomer was sprayed onto the surface of the first layer. To prepare the second layer, the ink consisting of PtRu black catalyst (Johnson Matthey) and Nafion ionomer was prepared using the same method as described above and then brushed onto the first layer at 60 °C. The resulting PtRu black catalyst loading was 2.5 mg cm⁻² and the Nafion content was 15 wt.%. The other D-L anode catalyst layer (denoted as D-L-2 anode catalyst layer) was prepared by the reverse order. For comparison, two anodes with S-L catalyst layers were also pre-
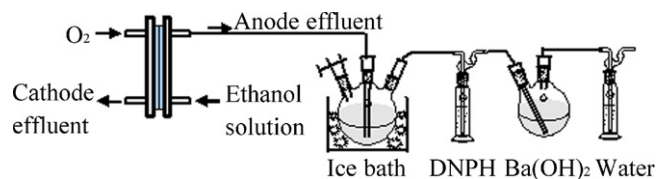

Fig. 1. Set-up for trapping the anode outlet products of DEFC.

pared in the same way. The S-L Pt₃Sn/C catalyst layer has the same catalyst and Nafion loading as the first layer in the D-L-1 anode, and finally 1 mg cm⁻² dry Nafion ionomer was sprayed onto the surface of the catalyst layer. The PtRu black loading was 6 mg cm⁻² and the Nafion content was 15 wt.% in the S-L PtRu black catalyst layer. In all cases, the identical cathode catalyst layers were prepared by brushing cathode ink onto the cathode diffusion layer held on a heating table at 60 °C. The resulting Pt loading was 3.7 mg cm⁻² and the Nafion content was 12 wt.%. Finally, anode and cathode (2 cm × 2 cm) were placed onto the two sides of the Nafion® 115 membrane and hot-pressed at 135 °C and 2000 pounds for 2 min to form the MEA.

2.3. Analysis of catalysts and MEAs

X-ray diffraction (XRD) patterns were recorded with a Rigaku Rotalflex (RU-2000B) X-ray diffractometer using Cu Kα radiation with a Ni filter. The tube current was 100 mA with a tube voltage of 40 kV. The 2θ angular regions between 15° and 85° were explored at a scan rate of 5° min⁻¹. Catalyst morphology was investigated by a TECNAI F30 transmission electron microscopy (FEI Corp.). The cross-sectional morphology of the D-L-1 anode catalyst layer was examined by JEOL JSM-5600LV SEM.

2.4. Single cell test and linear sweep voltammetry (LSV) measurement

The MEA was fitted between two stainless steel plates in a punctual flow bed [20]. The polarization curves were obtained using a Fuel Cell Test System (Arbin Instrument Corp.) under the operation conditions of 90 °C, 1 mL min⁻¹ of 1.5 mol L⁻¹ ethanol solution and non-humidified oxygen at a pressure of 0.2 MPa and a flow rate of 240 mL min⁻¹. The LSVs of the anode catalyst layer were performed at 90 °C using an EG&G PAR 273 potentiostat at a scan rate of 1 mV s⁻¹. In this measurement, the anode was fed with 1.5 mol L⁻¹ ethanol solution at a flow rate of 1 mL min⁻¹ as the working electrode, and the cathode was fed with hydrogen gas as the counter and pseudo-reference electrode (dynamic hydrogen electrode, DHE) [21]. The hydrogen pressure and flow rate was 0.1 MPa and 50 mL min⁻¹, respectively.

2.5. Analysis of anode product

Fig. 1 presents the set-up for trapping the outlet products, which is a bit different from reference [15]. The DEFC was
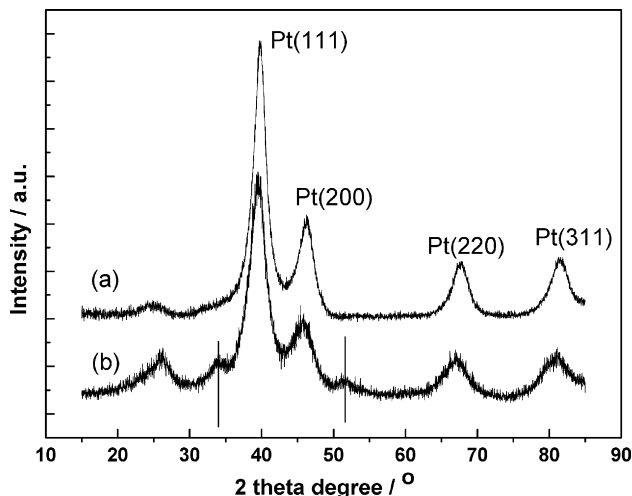
Fig. 2. X-ray diffraction patterns of (a) Pt/C and (b) Pt_3Sn/C catalysts.

operated at a certain cell voltage for 3 h under the operation conditions of 90 °C, 1 mL min^{-1} of 1.5 mol L^{-1} ethanol solution and non-humidified oxygen at a pressure of 0.2 MPa and a flow rate of 240 mL min^{-1}. The first flask was bathed in ice to reduce the volatility of the DEFC anode outlet solution. Acetaldehyde and CO_2 were adsorbed by saturated 2,4-dinitrophenylhydrazine (DNPH) in a 2.0 mol L^{-1} HCl solution and $Ba(OH)_2$ solution, respectively. In this experiment, no precipitation in DNPH solution was observed during the discharge process, which indicated that no acetaldehyde was volatilized from the first flask. Then 20 mL of the anode product was taken out from the first flask for gas chromatogram and titration analysis, the concentration of ethanol, acetaldehyde and ethyl acetate was determined by VARIAN CP-3800 gas chromatogram, and the concentration of acetic acid was titrated by standardized NaOH solution. The excess solution in the first flask was purged by pure nitrogen at a suitable flow rate for 2 h and then the CO_2 dissolved in the solution was adsorbed by the saturated $Ba(OH)_2$ solution in the second flask.

3. Results and discussion

The XRD patterns of Pt_3Sn/C and Pt/C catalysts were shown in Fig. 2. It could be seen that the Pt_3Sn/C catalyst displayed two small diffraction peaks of $SnO_2(1\,0\,1)$ and $SnO_2(2\,1\,1)$ at around 34° and 52°, respectively, which were apart from the four diffraction peaks of Pt(1 1 1), Pt(2 0 0), Pt(2 2 0), and Pt(3 1 1) (PCPDF#411445, #040802) [22]. It could also be observed that Pt related diffraction peaks on Pt_3Sn/C catalyst shifted to lower angles compared with Pt/C catalyst, which indicated that Pt_3Sn alloy was formed. The mean particle diameter of the catalyst was 2.38 nm calculated from Scherrer equation with Pt(2 2 0) diffraction peak [23], which was corresponding to the result of Fig. 3. The lattice parameter of the catalyst was 3.951 Å according to the Vegard's law [23], which is larger than that of Pt/C (3.915 Å), suggesting that the lattice of Pt in the Pt_3Sn/C catalyst is dilated when Sn atom joins. From our previous work [7], it could be concluded that Pt_3Sn/C catalyst with a suitable ratio
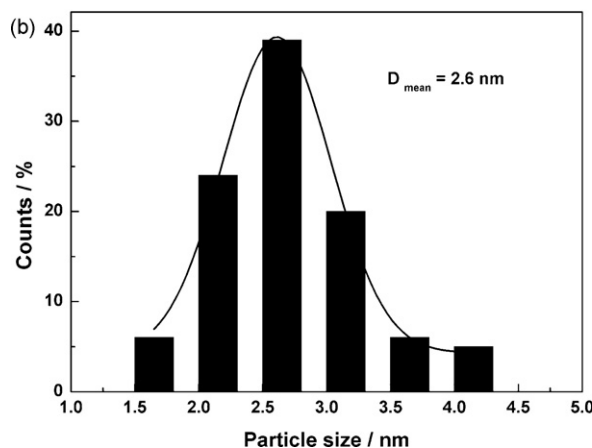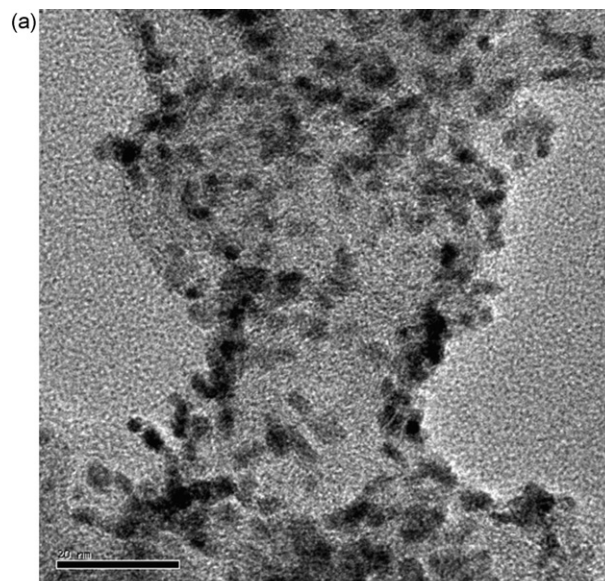

Fig. 3. TEM image (a) and the corresponding histogram of particle size distribution (b) of Pt_3Sn/C catalyst.

of PtSn alloy and tin oxide would display an optimum ethanol electro-oxidation activity although the ratio was not very clear. Fig. 3(a) and (b) showed the TEM image and the corresponding histogram of particle size distribution of in-house Pt_3Sn/C catalyst, respectively. It could be seen that the metal particles were uniformly distributed on the support and had a narrow distribution with the mean particle size of 2.6 nm.

Fig. 4 showed single cell performances of DEFC with D-L-1 and D-L-2 anode catalyst layers, S-L PtRu black and Pt_3Sn/C catalyst layers, respectively. It could be clearly seen that the open circuit voltage (OCV) of DEFC with two S-L catalyst layers was quite different, which was about 0.71 V and 0.86 V for S-L PtRu black and Pt_3Sn/C catalyst layer, respectively. In the case of DEFC with S-L Pt_3Sn/C catalyst layer, the higher OCV could be attributed to its negative shift of onset potential for ethanol electro-oxidation (discussed in the next paragraph). In the low current density region (<200 mA cm^{-2}), i.e. at low anode over-potential, the cell voltage of DEFC with S-L Pt_3Sn/C catalyst layer was much higher than that of DEFC with S-L PtRu black catalyst layer. However, it declined more speedily in the high
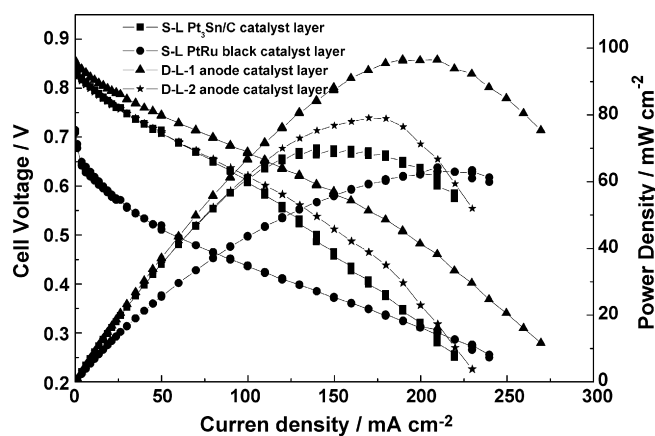
Fig. 4. Comparison of DEFC single cell performance with different anode catalyst layers under the operation conditions of 90 °C, 1 mL min^{-1} of 1.5 mol L^{-1} ethanol solution and non-humidified oxygen at a pressure of 0.2 MPa and a flow rate of 240 mL min^{-1}.

current density region. The DEFC with S-L PtRu black catalyst layer, on the contrary, showed its advantage when the current density was greater than 200 mA cm^{-2}, where the anode was deeply polarized. Due to their different superiorities, the maximum power density of DEFC with S-L PtRu black catalyst layer was only a little lower than that of DEFC with S-L Pt$_3$Sn/C catalyst layer (about 63 mW cm^{-2} and 70 mW cm^{-2}, respectively). When the anode catalyst layer was replaced by two D-L anode catalyst layers, the advantages of both PtRu black and Pt$_3$Sn/C catalyst layer appeared and the cell voltage increased in both low and high current density regions, the DEFC with D-L-1 and D-L-2 anode catalyst layers showed a maximum power density of 96 mW cm^{-2} and 79 mW cm^{-2}, respectively. The performance difference between the two D-L anode catalyst layers was probably ascribed to the electrode structure. Fig. 5 showed the cross-sectional SEM image of the D-L-1 anode catalyst layer. It could be seen that the two catalyst layers are separated clearly with an average thickness of 8.2 μm for the PtRu black catalyst layer on the top of membrane and an average thickness of 53 μm for the PtSn/C catalyst layer adjacent to the anode diffusion layer. Compared with the PtRu black catalyst layer, the Pt$_3$Sn/C catalyst layer was more porous and hydrophobic due
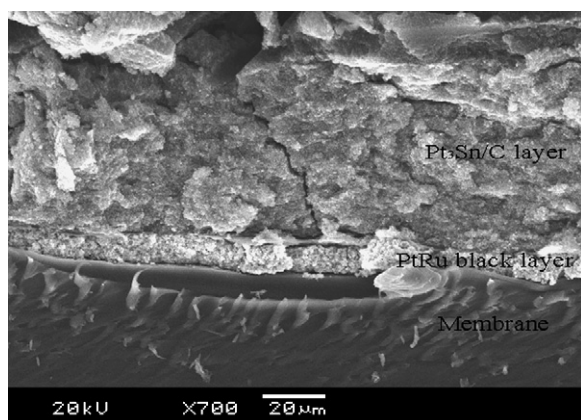

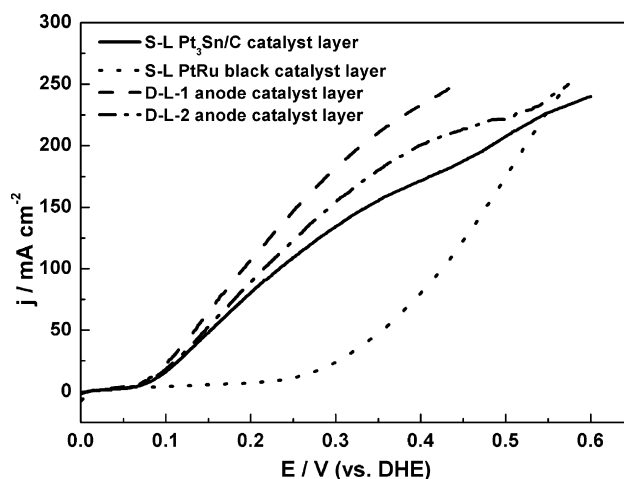Fig. 5. Cross-sectional SEM image of D-L-1 anode catalyst layer.

Fig. 6. Anode polarization curves of DEFC with different anode catalyst layers at 90 °C, recorded at a scan rate of 1 mV/s. The anode was fed with 1.5 mol L^{-1} ethanol solution at a flow rate of 1 mL min^{-1}, and the cathode was fed with 0.1 MPa hydrogen at a flow rate of 50 mL min^{-1}.

to the high content of carbon black, so the configuration in the D-L-1 anode catalyst layer was more favourable for the transportation of the reactants and products at the anode than that in the D-L-2 anode catalyst layer, which resulted in a higher performance.

To further clarify the reasons for the improvement of DEFC performance with D-L anode catalyst layers, anode polarization curves for the four single cells were measured as shown in Fig. 6. The maximum polarization potential was set at 0.6 V in order to prevent the dissolution of Sn, and the current limit is 1 A in the potentiostat. The faradic current was normalized by the geometrical electrode area. The profiles showed clearly that the onset of ethanol electro-oxidation on the DEFC with two D-L anode catalyst layers and S-L Pt$_3$Sn/C catalyst layer was all about 0.08 V, while the reaction commenced at 0.25 V on the DEFC with S-L PtRu black catalyst layer. The result indicated that the S-L Pt$_3$Sn/C and two D-L anode catalyst layers revealed better ethanol electro-oxidation activities at low anode polarization potentials, which was in good agreement with the results obtained from Fig. 4. When the anode polarization potential further increased, the difference in current density between D-L-1 anode catalyst layers and S-L Pt$_3$Sn/C catalyst layer increased more and more. In the case of DEFC with S-L PtRu black catalyst layer, the current density increased more rapidly than the others after the onset, and was greater than that in S-L Pt$_3$Sn/C catalyst layer when the anode polarization potential was larger than 0.55 V. Therefore, the S-L PtRu black and Pt$_3$Sn/C catalyst layers exhibited their superiorities at different anode polarization potential regions. It is very interesting to note that the two D-L anode catalyst layers revealed the combined effects of PtRu and PtSn catalysts, and thus showed higher ethanol electro-oxidation activities than S-L PtRu black and Pt$_3$Sn/C catalyst layers in the entire polarization potential region. Corresponding to the result of Fig. 4, the D-L-1 anode catalyst layer also showed a greater performance than the D-L-2 anode catalyst layer in the anode polarization curve, so more attention was paid to the D-L-1 anode catalyst layer in the next paragraph.

Table 1
The product concentration, product yield and current efficiency of acetaldehyde (AAL), ethyl acetate (EA), acetic acid (AA) and CO_2, formed in DEFC with the D-L-1, S-L Pt_3Sn/C and PtRu black anode catalyst layers, respectively

		Anode								
		D-L-1			Pt_3Sn/C			PtRu black		
		0.6^a	0.5^a	0.4^a	0.6^a	0.5^a	0.4^a	0.6^a	0.5^a	0.4^a
Product concentration (mmol L^{-1})	AAL	13.64	22.95	25.45	9.32	12.95	21.14	28.18	45.68	50.45
	EA	4.20	4.77	3.86	3.52	2.84	2.95	3.86	3.64	4.09
	AA	232	273	317	204	233	262	110	138	224
	CO_2	0.34	1.3	1.64	0.19	0.44	0.81	0.32	0.80	1.80
Product yield (%)	AAL	5.45	7.60	7.31	4.29	5.20	7.37	19.79	24.28	18.00
	EA	1.68	1.58	1.11	1.62	1.14	1.03	2.71	1.93	1.46
	AA	92.73	90.39	91.11	94.00	93.48	91.32	77.27	73.36	79.90
	CO_2	0.14	0.43	0.47	0.09	0.18	0.28	0.23	0.43	0.64
Current efficiency (%)	AAL	2.79	3.92	3.76	2.19	2.66	3.80	10.92	13.68	9.75
	EA	1.72	1.63	1.14	1.65	1.17	1.06	3.0	2.18	1.58
	AA	95.06	93.12	93.65	95.88	95.62	94.27	85.32	82.69	86.59
	CO_2	0.43	1.33	1.45	0.27	0.55	0.87	0.76	1.45	2.08

^a Cell voltage (V).

Based on the previous works [6,11,14,24–30], ethanol electro-oxidation in acid solution could be summarized as two parallel reaction pathways. One pathway was the cleavage of C–C bond to form CO_2, and the other was a 'direct' oxidation pathway to form acetaldehyde and acetic acid. Table 1 listed the anode product distributions and current efficiencies of DEFC with D-L-1 anode catalyst layer, S-L Pt_3Sn/C catalyst layer and S-L PtRu black catalyst layer under different cell voltages. It could be seen from Table 1 that acetaldehyde, acetic acid, ethyl acetate and CO_2 were detected in the DEFC anode effluent, and C2 species were the major anode products. However, the yields and current efficiencies of the anode products were different in the DEFC with different anode catalyst layers. For example, when the cell voltage was 0.5 V, the yield of acetic acid in the DEFC with S-L PtRu black, S-L Pt_3Sn/C and D-L-1 anode catalyst layers was 73.36%, 93.48% and 90.39%, and the corresponding current efficiency was 82.69%, 95.62% and 93.12%, respectively. In the case of acetaldehyde, the product yield of DEFC with D-L-1 anode catalyst layer varied almost the same with that of DEFC with S-L Pt_3Sn/C catalyst layer (<10%), both obviously less than that of DEFC with S-L PtRu black catalyst layer (about 20%). It could also be seen that CO_2 yield increased with current density, indicating that more C–C bonds were broken when the anode overpotential of DEFC increased. At each cell voltage, CO_2 yield of DEFC with S-L Pt_3Sn/C catalyst layer displayed least, while the formation of CO_2 was easier in DEFC with D-L-1 anode catalyst layer, similar to that of DEFC with S-L PtRu black catalyst layer. So, the DEFC with D-L-1 anode catalyst layer not only favored the C–C bond splitting, resulting in the formation of CO_2, but also contributed to the formation of C2 species, including acetic acid and acetaldehyde.

Based on the analysis from Table 1, we calculated the ethanol oxidation efficiencies according to the following formula (Eq. (1)), as shown in Fig. 7.

$$\eta = \frac{(0.5 \times M_{CO_2} + 2 \times M_{EA} + M_{AAL} + M_{AA}) \times V_{out}}{M_{ethanol}^0 \times V_{in}} \times 100\%$$

(1)

where η was the ethanol oxidation efficiency, M_{CO_2}, M_{EA}, M_{AAL} and M_{AA} was the concentration of CO_2, ethyl acetate, acetaldehyde and acetic acid, respectively, $M_{ethanol}^0$ was the initial concentration of ethanol, V_{out} and V_{in} was the volume of inlet and outlet solution in the anode of the DEFC, respectively. It could be concluded from Fig. 7 that ethanol oxidation efficiency increased as cell voltage decreased because there was more ethanol oxidized with the increasing of current density. Compared with the S-L Pt_3Sn/C and PtRu black catalyst layers, the oxidation efficiencies were higher at all the studied cell voltages on DEFC with the D-L-1 anode catalyst layer, which resulted in a higher performance.
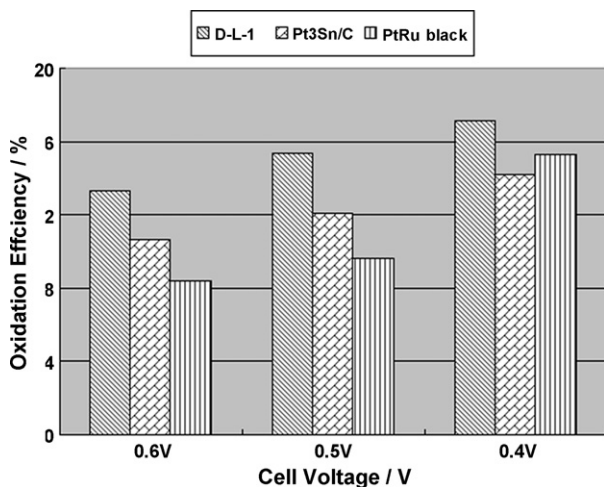

Fig. 7. Ethanol oxidation efficiencies for DEFC with different anode catalyst layers at 90 °C.

4. Conclusion

DEFC performance was improved by fabricating novel D-L anode catalyst layers with two reverse configurations using in-house 45 wt.% PtSn/C catalyst and commercial PtRu black catalyst. XRD and TEM characterization results indicated that the in-house Pt_3Sn/C catalyst was alloyed partially and that the metal particles were uniformly distributed on the support with a mean particle size of 2.6 nm. Due to the favorable electrode structure, the DEFC with D-L anode catalyst layer in the order of PtSn/C and PtRu black catalyst layers from the anode diffusion layer showed a higher performance than that with D-L anode catalyst layer in the reverse order. The maximum power density of DEFC with this favorable D-L anode catalyst layer was 96 mW cm^{-2} under the operation conditions of 90 °C, 1 mL min^{-1} of 1.5 mol L^{-1} ethanol solution and non-humidified oxygen at a pressure of 0.2 MPa and a flow rate of 240 mL min^{-1}, which increased by 52.4% and 37.1% compared with DEFC with S-L PtRu black and PtSn/C catalyst layers, respectively. Anode polarization curves suggested that the D-L anode catalyst layers performed higher ethanol electro-oxidation activities than S-L PtRu black and Pt_3Sn/C catalyst layers. The analysis of DEFC anode products indicated that acetic acid was the major product with the product yield and current efficiency larger than 70% and 80%, respectively, while CO_2 as the least product with the maximum current efficiency of about 2.08%. In addition, the yield of acetic acid in DEFC with D-L anode catalyst layer was similar to that in DEFC with S-L PtSn/C catalyst layer, and the yield of CO_2 in DEFC with D-L anode catalyst layer was close to that in DEFC with S-L PtRu black catalyst layer. These results suggested that the DEFC with D-L anode catalyst layer possessed the advantages of both PtRu black and Pt_3Sn/C catalysts, and thus showed higher product yields, current efficiencies and ethanol oxidation efficiencies than those with S-L PtRu black and Pt_3Sn/C catalyst layers.

Acknowledgements

References

[1] F. Delime, J.M. Leager, C. Lamy, J. Appl. Electrochem. 28 (1998) 27.
[2] W.J. Zhou, Z.H. Zhou, S.Q. Song, W.Z. Li, G.Q. Sun, P. Tsiakaras, Q. Xin, J. Appl. Catal. B: Environ. 46 (2003) 273.
[3] L.W. Leung, S.C. Chang, M.J. Weaver, J. Electroanal. Chem. 266 (1989) 317.
[4] N. Fujiwara, K.A. Friedrich, U. Stimming, J. Electroanal. Chem. 472 (1999) 120.
[5] F. Vigier, S. Rousseau, C. Coutanceau, J. Leger, C. Lamy, Top. Catal. 40 (2006) 111.
[6] Z. Jusys, J. Kaiser, R.J. Behm, Phys. Chem. Chem. Phys. 3 (2001) 4650.
[7] L. Jiang, G. Sun, S. Sun, J. Liu, S. Tang, H. Li, B. Zhou, Q. Xin, Electrochim. Acta 50 (2005) 5384.
[8] F. Vigier, C. Coutanceau, F. Hahn, E.M. Belgsir, C. Lamy, J. Electroanal. Chem. 563 (2004) 81.
[9] Z.L. Liu, X.Y. Ling, X.D. Su, J.Y. Lee, L.M. Gan, J. Power Sources 149 (2005) 1.
[10] X.S. Zhao, L.H. Jiang, G.Q. Sun, S.H. Yang, B.L. Yi, Q. Xin, Chin. J. Catal. 25 (2004) 983.
[11] G.A. Camara, R.B. de Lima, T. Iwasita, J. Electroanal. Chem. 585 (2005) 128.
[12] L. Jiang, Z. Zhou, W. Li, W. Zhou, S. Song, H. Li, G. Sun, Q. Xin, Energy Fuels 18 (2004) 866.
[13] F. Colmati, E. Antolini, E.R. Gonzalez, J. Power Sources 157 (2006) 98.
[14] C. Lamy, S. Rousseau, E.M. Belgsir, C. Coutanceau, J.M. Leger, Electrochim. Acta 49 (2004) 3901.
[15] S. Rousseau, C. Coutanceau, C. Lamy, J.M. Leger, J. Power Sources 158 (2006) 18.
[16] Q. Wang, G.Q. Sun, L.H. Jiang, Q. Xin, S.G. Sun, Y.X. Jiang, S.P. Chen, Z. Jusys, R.J. Behm, Phys. Chem. Chem. Phys. 9 (2007) 2686.
[17] H. Wang, Z. Jusys, R.J. Behm, J. Power Sources 154 (2006) 351.
[18] L.H. Jiang, G.Q. Sun, Z.H. Zhou, Q. Xin, Catal. Today 93–95 (2004) 665.
[19] G.X. Wang, G.Q. Sun, Z.H. Zhou, J.G. Liu, Q. Wang, S.L. Wang, J.S. Guo, S.H. Yang, Q. Xin, B.L. Yi, Electrochem. Solid-State Lett. 151 (2005) A12–A16.
[20] S. Song, G. Wang, W. Zhou, X. Zhao, G. Sun, Q. Xin, S. Kontou, P. Tsiakaras, J. Power Sources 140 (2005) 103.
[21] H.N. Dinh, X.M. Ren, F.H. Garzon, P. Zelenay, S. Gottesfeld, J. Electroanal. Chem. 491 (2000) 222.
[22] JCPDS, International Centre for Diffraction Data, 1987.
[23] V. Radmilovic, H. Gasteiger, P. Ross, J. Catal. 154 (1995) 98.
[24] B. Beden, M.C. Morin, F. Hahn, C. Lamy, J. Electroanal. Chem. 229 (1987) 353.
[25] P. Gao, S.C. Chang, Z. Zhou, M.J. Weaver, J. Electroanal. Chem. 272 (1989) 161.
[26] J.M. Perez, B. Beden, F. Hahn, A. Aldaz, C. Lamy, J. Electroanal. Chem. 262 (1989) 251.
[27] T. Iwasita, B. Rasch, E. Cattaneo, Electrochim. Acta 34 (1989) 1073.
[28] T. Iwasita, E. Pastor, Electrochim. Acta 39 (1994) 531.
[29] X.H. Xia, H.-D. Liess, T. Iwasita, J. Electroanal. Chem. 437 (1997) 233.
[30] L. Colmenares, H. Wang, Z. Jusys, L. Jiang, S. Yan, G.Q. Sun, R.J. Behm, Electrochim. Acta 52 (2006) 221.